

Article

Structure of the Pacific Walker Circulation Depicted by the Reanalysis and CMIP6

Emmanuel Olaoluwa Eresanya^{1,2,3}  and Yuping Guan^{1,2,4,*}

¹ State Key Laboratory of Tropical Oceanography, South China Sea Institute of Oceanology, Chinese Academy of Sciences, Guangzhou 510301, China; eresanyaemmanuel44@gmail.com

² College of Marine Sciences, University of Chinese Academy of Sciences, Beijing 100049, China

³ Department of Marine Science and Technology, Federal University of Technology, Akure P.M.B. 704, Nigeria

⁴ Southern Marine Science and Engineering Guangdong Laboratory (Guangzhou), Guangzhou 511458, China

* Correspondence: guan@scsio.ac.cn

Abstract: The Pacific Walker circulation (PWC) is one of the most important components of large-scale tropical atmospheric circulations. The PWC and its influences have been studied extensively by numerical models and reanalysis. The newly released ERA5 and NCEP2 are the most widely used reanalysis datasets and serve as benchmarks for evaluation of model simulations. If the results of these datasets differ significantly, this could lead to a bias in projected long-term climate knowledge. For better understanding of future climate change, it is necessary to evaluate PWC reanalysis productions. As a result, we compared the PWC structures between the ERA5 and NCEP2 datasets from month to seasonal time scales. We used the zonal mass streamfunction (ZMS) over the equatorial Pacific to indicate the strength of the PWC. The PWC's average monthly or seasonal cycle peaks around July. From February to June, the NCEP2 shows a higher PWC intensity, whereas the ERA5 shows greater intensity from July to December. The circulation center in the NCEP2 is generally stronger and wider than in the ERA5. The ERA5, however, revealed that the PWC's west edge (zero line of ZMS over the western Pacific) had moved 10 degrees westward in comparison to the NCEP2. In addition, we compared the PWC mean state in the reanalysis and CMIP6 models; the mean state vertical structures of the tropical PWC in the CMIP6 multi-model ensemble (MME) are similar to those of the reanalyses in structure but weaker and wider than in the two reanalysis datasets. The PWC is broader in CMIP6, and the western boundary is 7 and 17 degrees farther west than in the ERA5 and NCEP2, respectively. This study suggests that, when using reanalysis datasets to evaluate PWC structural changes in intensity and western edge, extreme caution should be exercised.

Keywords: Pacific Walker circulation; zonal mass streamfunction; structural changes; reanalysis datasets



Citation: Eresanya, E.O.; Guan, Y. Structure of the Pacific Walker Circulation Depicted by the Reanalysis and CMIP6. *Atmosphere* **2021**, *12*, 1219. <https://doi.org/10.3390/atmos12091219>

Academic Editor: Indrani Roy

Received: 19 August 2021

Accepted: 15 September 2021

Published: 17 September 2021

Publisher's Note: MDPI stays neutral with regard to jurisdictional claims in published maps and institutional affiliations.



Copyright: © 2021 by the authors. Licensee MDPI, Basel, Switzerland. This article is an open access article distributed under the terms and conditions of the Creative Commons Attribution (CC BY) license (<https://creativecommons.org/licenses/by/4.0/>).

1. Introduction

The Pacific Walker circulation (PWC) is an important component of the global climate system; it features low-level winds blowing from east to west across the central Pacific, a rising motion over the Maritime Continent and the warm western Pacific, returning flow from west to east in the upper troposphere, and a sinking motion over the cold water of the eastern Pacific [1–6]. The PWC regulates the global exchange of heat energy, momentum, and water vapor within the tropics through substantial overturning motions. It performs a major task in the steadiness of atmospheric energy. The state and variability of the PWC have huge socio-economic significance. Its importance in understanding weather and climate accurately has inspired several studies on its dynamics [7], variability [8], and trends [9].

Many studies have used the zonal mass streamfunction (ZMS) to investigate variations in the PWC [8,10–12]. A consensus from studies on the PWC dynamics and variation is the respective strengthening and weakening in the west and east Pacific in recent

decades [8,10,12–20]. Its variation is closely linked to the El Niño Southern Oscillation (ENSO), the monsoonal circulation, and rainfall over adjacent continents [2,9,21]. The PWC intensity and structure have changed over time in response to changes in precipitation and temperature, such as the drying of eastern Africa, intensified Northern Hemisphere summer monsoon precipitation, and a recent global warming hiatus [15,21–28].

By using seven sets of reanalysis data (1979–2012), Ma and Zhou [10] evaluated and compared the long-term linear trends of the PWC and found varying degrees of strengthening and a westward moving trend of the PWC. Previous research on the PWC changes focused on long-term projections [10,29–31], paying little attention to monthly or seasonal behaviors. If a climate model cannot capture these basic features, the projection of the long-term future climate change would induce a large bias. However, considering the variation among these datasets and their biases compared with climate models, whether these PWC developments and the variation derived from these reanalysis data imitate those in reality are uncertain [32,33].

The long-term changing trend in the PWC is not consistent with climate models. Previous studies have revealed a considerable inconsistency over the equatorial Pacific in the reanalysis from models [34,35]. The biases between reanalysis and climate models may distort the real variation and produce flawed outcomes. Because the zonal and meridional wind are directly assimilated from observational data, the atmospheric circulation in a reanalysis dataset is the best estimate of real atmospheric circulation [36]. NCEP and ERA are the most commonly used reference or benchmark datasets for evaluating climate models using reanalysis datasets [27,37].

To depict the PWC, it is necessary to understand the differences between results of NCEP and ERA. In this study, we investigated the PWC change features, including the intensity and western edge from monthly to seasonal time scales and compared the results indicated by ERA5 and NCEP2 datasets. Furthermore, we compared the mean state vertical structures and the western edge of the tropical PWC in the reanalysis and CMIP6 models. The following is how this paper is organized. The datasets and methods used are discussed in Section 2. In Section 3, we compare ERA5 and NCEP2 reanalysis data and look into long-term changes in the PWC features in both the reanalysis and the CMIP6 models. The summary and discussion are found in Section 4, and the conclusion is found in Section 5.

2. Datasets

2.1. Observations

Forty-one years (1979–2019) of monthly vertical velocity (ω), u , and v wind datasets of the National Centers for Environmental Prediction NCEP–U.S. Department of Energy reanalysis (NCEP-2; [38], <http://www.esrl.noaa.gov/psd/data/gridded/data.ncep%20.reanalyses2.html> (accessed on 14 September 2021) and the fifth generation ECMWF reanalysis for the global climate and weather (Era5; [39,40] <https://cds.climate.copernicus.eu/cdsapp#!/home> accessed on 14 September 2021) over the Tropical Pacific (20° S–20° N, 80° E–280° E) were used in this study. Results of reanalysis datasets imitate their original spatial resolutions.

2.2. CMIP6 Models

To examine the changes of the PWC, we used nine (9) models (listed in Table 1) that are part of the Coupled Model Intercomparison Project (CMIP) Phase 6 [41]. The first ensemble member (i.e., r1i1p1f1) run for each model in the same period from 1979 to 2014 was used in this study. All model data are replotted onto a common $2.5^\circ \times 2.5^\circ$ horizontal grid using bilinear interpolation before the analyses.

Table 1. Description of the nine CMIP6 models used in the study. Horizontal resolution shows the number of grid points in the meridional by zonal directions.

S/N	Model Name	Horizontal Resolution (°)	Institute
1.	BCC-CSM2-MR	320 × 160	Beijing Climate Center, China Meteorological Administration, China
2.	BCC-ESM1	128 × 64	Beijing Climate Center, China Meteorological Administration, China
3.	CanESM5	128 × 64	Canadian Centre for Climate Modelling and Analysis, Canada
4.	CESM2-WACCM	288 × 192	National Center for Atmospheric Research, USA
5.	E3SM-1-0	360 × 180	Energy Exascale Earth System Model (https://www.llnl.gov (accessed on 14 September 2021))
6.	GISS-E2-1-G	144 × 90	National Aeronautics and Space Administration- Goddard Institute for Space Studies
7.	GISS-E2-1-H	144 × 90	National Aeronautics and Space Administration- Goddard Institute for Space Studies
8.	MIROC6	256 × 128	Atmosphere and Ocean Research Institute, National Institute for Environmental Studies, and Japan Agency for Marine-Earth Science and Technology, Japan
9.	MRI-ESM2-0	320 × 160	Meteorological Research Institute, Japan

2.3. Methodology

To depict the PWC, we used the ZMS as its representation over the tropical Pacific (20° S–20° N, 80° E–280° E). As a measure for the zonal circulation along the equator, the zonal mass streamfunction is defined in Equation (1) [8].

$$\psi = 2\pi a \int_0^p u_D \frac{dp}{g} \quad (1)$$

where ψ is the zonal mass streamfunction, u_D is the divergent component of the zonal wind, a is the radius of the earth, p is the pressure, and g is the gravitational acceleration.

The divergent component of the zonal wind was calculated by computing the Poisson equation for the potential function with divergence as the driving term, and then computing the divergent component of zonal wind (u_D). u_D was then averaged over a 5° N to 5° S meridional band and integrated from the top of the atmosphere to the surface. We only showed the levels below 100 hPa in our figures because the zonal mass streamfunction was approximately zero above that level. To guarantee the reliability of results, we considered the available dataset from 1979 to 2019. The strength of the PWC is defined as the vertically and zonally averaged ZMS over the tropical Pacific, between 150° E and 120° W, the central area with a confident concrete intensity (Figure 1). The mean state was determined by taking the average of the entire research period (1979–2019).

To describe the state of the PWC cell, we defined the PWC west edge by the zero line of the vertically integrated ZMS on the west of the international dateline of all levels averaged. It is worth mentioning that the outcomes are dependent on the chosen pressure levels.

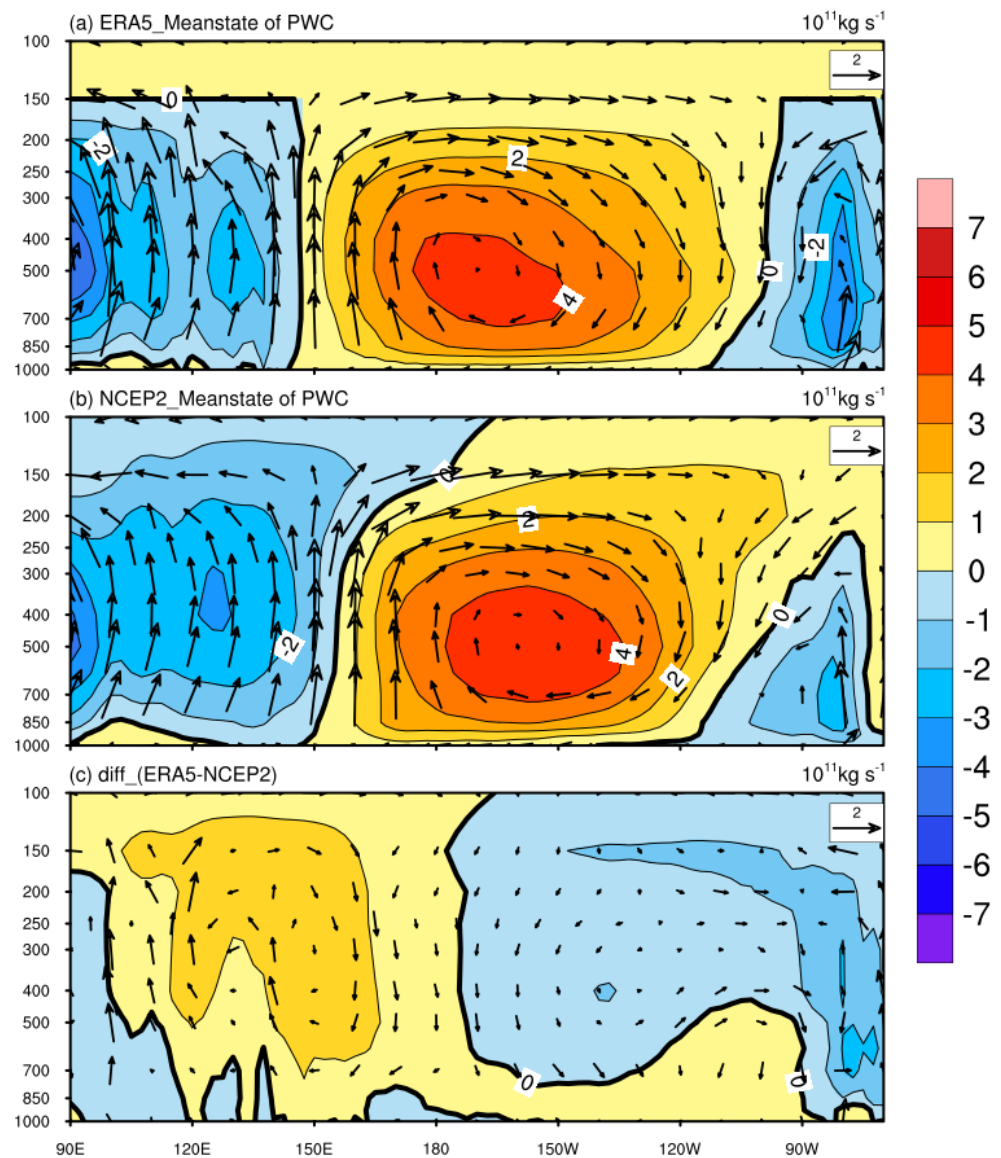


Figure 1. Mean state (1979–2019) of the tropical PWC in (a) ERA5, (b) NCEP2, and (c) difference (ERA5-NCEP2). Vectors are the composite of pressure velocity ($\omega x -50$; Pa s^{-1}) and zonal divergent wind (m s^{-1}). Shading and contours represent zonal mass streamfunction (10^{11} Kg/s) averaged between 5° S and 5° N .

2.4. Statistical Significance Evaluation of Trends

All of the parameters in this study had their trends computed using least-squares linear regressions, and their level of significance was determined using a two-tailed Student's t test (null hypothesis of zero linear trend) with an operational degree of freedom [42] similar to that in previous studies [23,26,43].

3. PWC Evolution and Variation in Recent Years

To better understand the evolution and variation in the PWC in recent years, we present the mean-state, monthly, and seasonal variation in the PWC using ZMS computed from ERA5 and NCEP2 reanalysis datasets from 1979 to 2019.

3.1. Long-Term Mean PWC Characteristics and Changes

In this section, we compare the mean state of the PWC. Figure 1 depicts the long-term mean annual zonal mass streamfunction (ZMS), corresponding zonal divergent winds, and vertical winds derived from ERA5 and NCEP2 reanalysis datasets along the equatorial

Pacific (5° S and 5° N). Since the atmospheric mass flux over 100 hPa is insignificant, the findings above 100 hPa are not displayed. The zonal atmospheric circulation is represented by alternating negative and positive cells in the ZMS. The PWC is the most robust full cell positioned east of the Maritime Continent, with positive (negative) values indicating clockwise (anticlockwise) rotation, which are steady with composite vectors of zonal divergent and vertical winds.

The PWC cell's core is near the equatorial central Pacific (between 170° W and 150° W), positioned in the middle troposphere (500 hPa). The denser constant streamfunction lines over the regions, approximately 150° E and 120° W, respectively, are consistent with stronger ascending motion over the Maritime Continent and western Pacific and descending motion over the eastern Pacific. The ZMS visualizes the entire structure of the PWC, which is characterized by an updraft center over the Maritime Continent and western Pacific, westerlies in the upper troposphere, a strong downdraft in the eastern Pacific, and surface easterlies, resulting in an enclosed cell, when combined with the results of the zonal divergent circulation.

The pattern of correlation of the ZMS over the equatorial Pacific is similar in PWC structural aspects assessed by the ERA5 and the NCEP2 (Figure 1). Nonetheless, there are slight discrepancies between the ERA5 and the NCEP2. In the NCEP2 (ERA5), for example, the PWC is stronger and wider (Figure 1b), with a ZMS of 5×10^{11} Kgs $^{-1}$ (4×10^{11} Kgs $^{-1}$) for the circulation center. In the ERA5, the western edge (zero line of ZMS over the western Pacific) and core of the PWC were farther west by 5° and 10° than in the NCEP2 (Figure 1a).

Figure 1c depicts the mean state difference between the ERA5 and the NCEP2 from 1979 to 2019. The western (eastern) Pacific is controlled by a positive (negative) ZMS. This indicates that the PWC intensity was weaker (stronger) in the ERA5 (NCEP2) reanalysis.

This is congruent with the results of Ma and Zhou [10], who found minor changes in the intensities and position of the PWC's western edge in different reanalysis datasets. Between 1979 and 2012, they used the ERAIM, JRA 25, JRA 55, MERRA, 20CR, NCEP1, and NCEP2 reanalysis datasets, and reported the highest (lowest) PWC intensity of 5.0×10^{11} Kgs $^{-1}$ (4.0×10^{11} Kgs $^{-1}$) in 20CR (MERRA).

We also conducted an integrated analysis of PWC changes using the zonal mass streamfunction, which accurately captures PWC structure aspects. Figure 2 depicts the ZMS's long-term trends in the equatorial Pacific from 1979 to 2019. In both reanalyses, the ZMS trends (shading) show quite a similar spatial pattern with respect to the long-term mean (contour), with a westward movement of the maximum positive ZMS trend center, compared to the climatological center of the PWC cell. The positive (negative) ZMS trends on the west (right) side of the PWC cell are both statistically significant at the 5% level, indicating an intensification and westward shift of the PWC in recent decades. Despite the great similarities in trend spatial patterns, there are also discrepancies in both reanalyses. For example, positive trends dominate the whole Pacific in the ERA5 (Figure 2a), whereas positive (negative) ZMS controls the west (east) Pacific in the NCEP2 (Figure 2b). ZMS's strong negative trends govern nearly all levels of the eastern Pacific, with the maximum center in the NCEP2's middle troposphere. In the NCEP2, the strongest negative trends dominate the eastern Pacific's low levels and extend westward toward the central Pacific, with a notable positive trend in the upper troposphere around the international dateline.

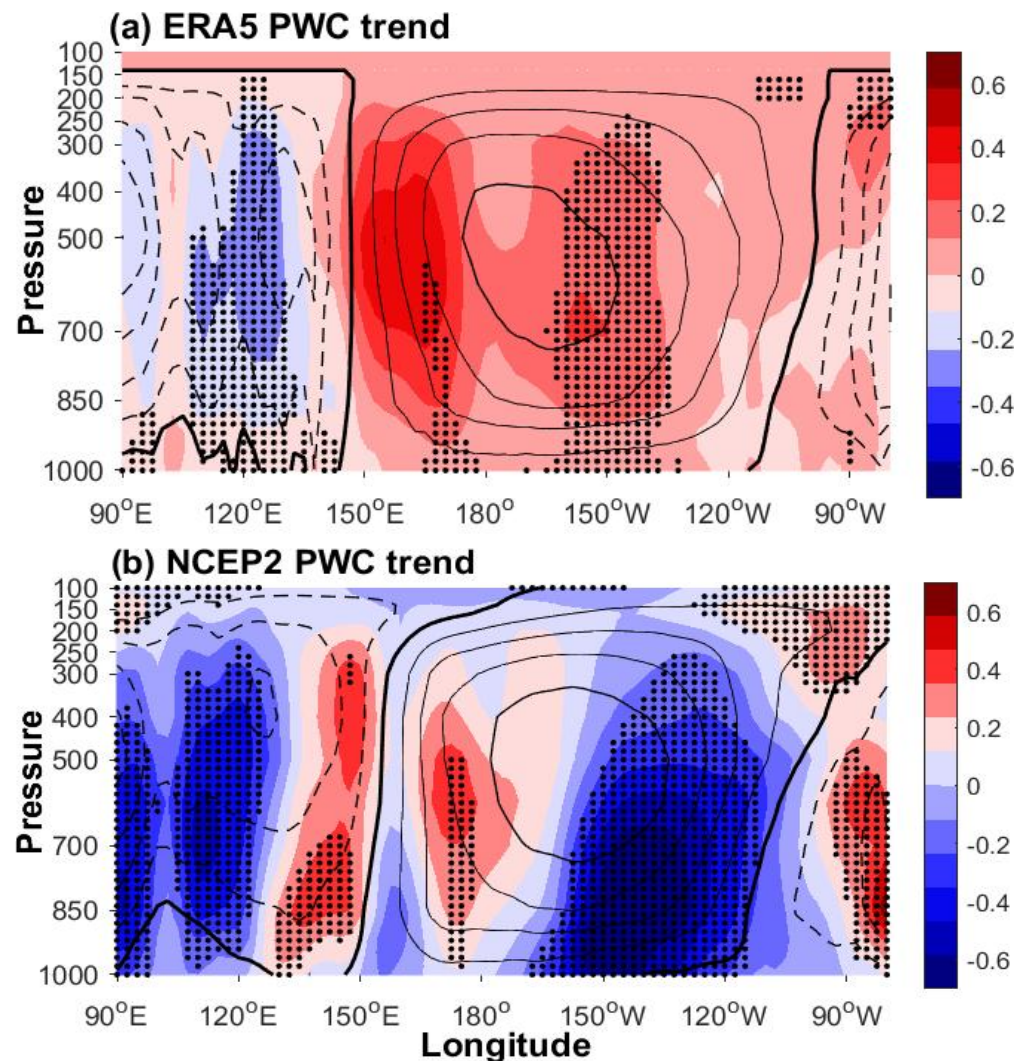


Figure 2. Long-term linear trends in the ZMS (shading: 10^{11} Kg/s/decade) of the tropical PWC in (a) ERA5 and (b) NCEP2, with trends that are statistically significant at the 5% level dotted. Contours denote the long-term mean of the zonal mass streamfunction.

3.2. The Monthly States of the PWC

The PWC is a zonal asymmetric tropical Pacific circulation that is driven by difference in sea surface temperature (SST) along the equatorial Pacific, which is caused by the continental disruption of foremost ocean motions over the Maritime Continent [2,3]. The PWC varies on a regular basis due to differences in the energy exchange between the atmosphere and the ocean [38,40]; consequently, we investigated the PWC's monthly evolution and alterations, as indicated by the ERA5 and the NCEP2.

In Section 3.1, we showed that the ERA5 and the NCEP2 have similar mean PWC patterns over the equatorial Pacific. Likewise, the monthly mean PWC variation revealed comparable patterns (Figure 3) in both reanalyses. The PWC was found to be stronger on the east Pacific in January and February, before shifting to the central Pacific in March and April. The PWC begins to increase westward in the west Pacific in May and continues until September, with a peak in July. The PWC begins to weaken in the west Pacific in October and continues to move eastward until December.

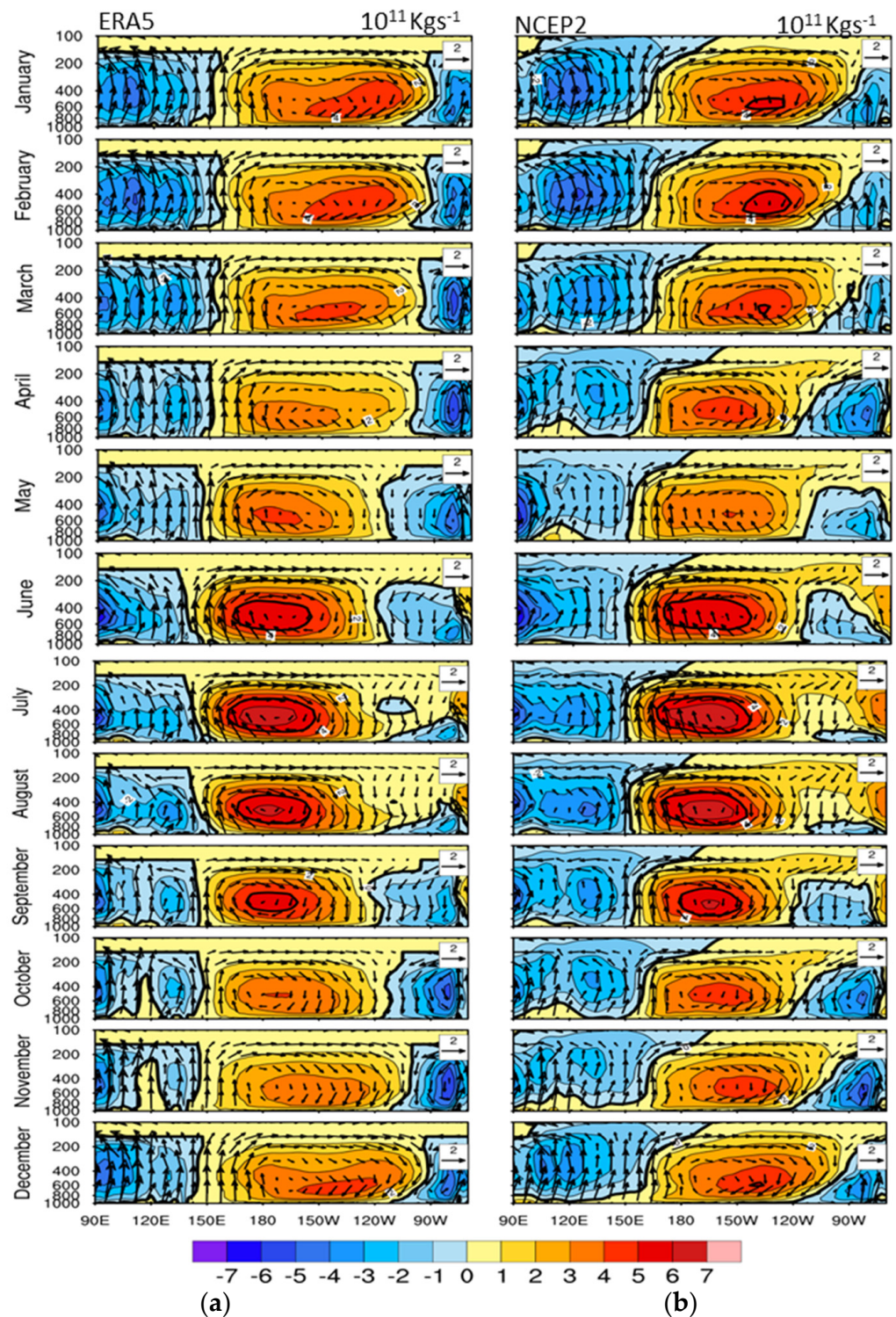


Figure 3. Monthly mean (1979–2019) variation in the tropical PWC in (a) ERA5 and (b) NCEP2. Vectors are the composite of pressure velocity ($\omega \times 50$; Pa s^{-1}) and zonal divergent wind (m s^{-1}). Shading and contours represent zonal mass streamfunction (10^{11} Kg/s) averaged between 5° S and 5° N .

Despite their similarity, the ERA5 and the NCEP2 have significant structural and longitudinal variances throughout the year. The NCEP2 revealed stronger and wider PWC core cells during both its peaks and low periods in April and June, respectively. The ERA5 revealed a small shift of nearly 10 degrees westward in the PWC core compared to

the NCEP2, most prominent in June to August. These variances are similar to the slight discrepancies observed in both reanalyses during the mean states reported earlier.

Figure 4 depicts the PWC climatological monthly mean difference of the ERA5 and the NCEP2 over the tropical Pacific. The intensity of the PWC changes slightly over the west and east Pacific across the months, with positive (negative) ZMS over the western (eastern) Pacific.

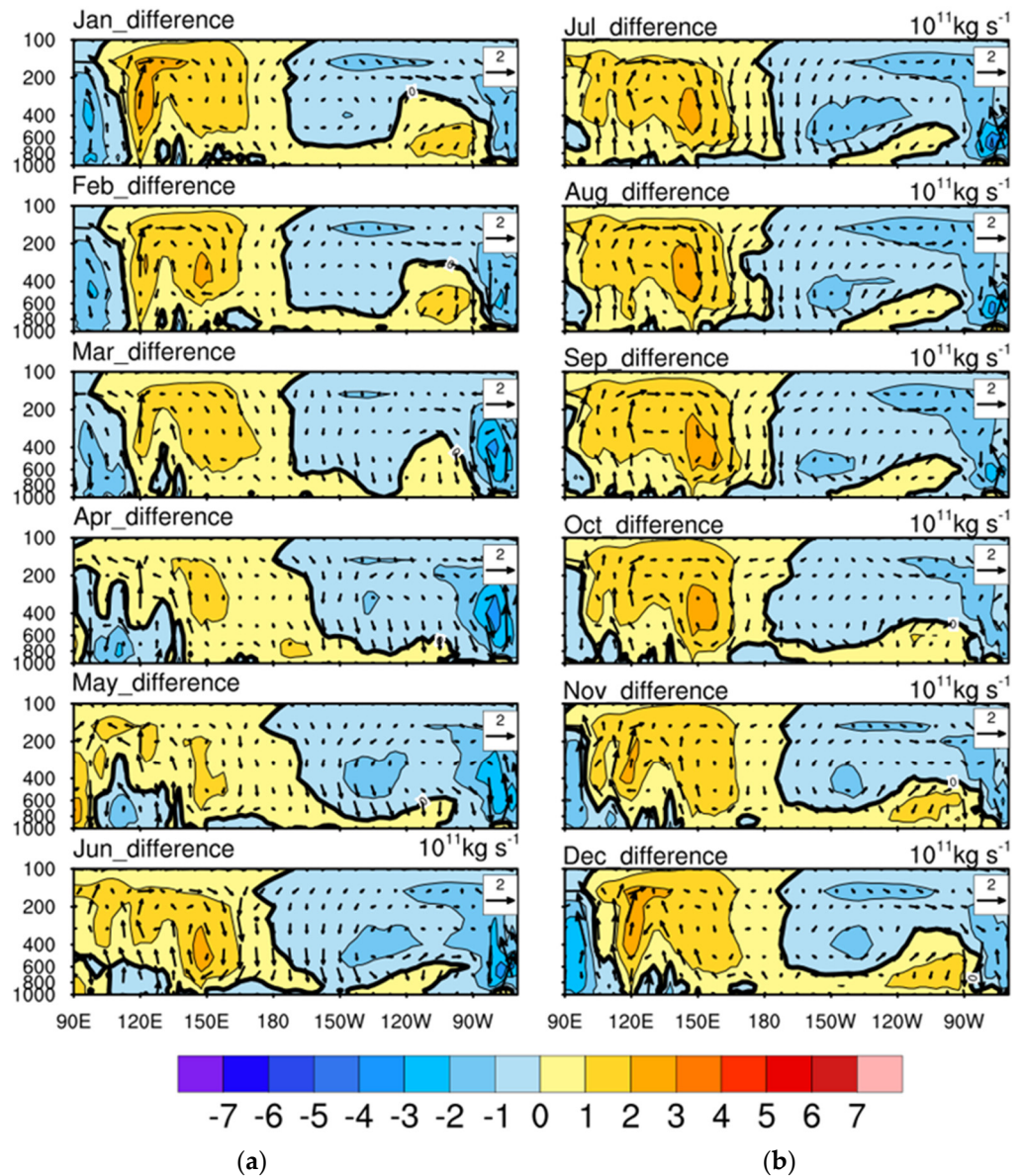


Figure 4. Monthly mean difference (1979–2019) of ERA5 and NCEP2. Vectors are the composite of pressure velocity ($\omega \times 50$; Pa s^{-1}) and zonal divergent wind (m s^{-1}). Shading and contours represent zonal mass streamfunction (10^{11} Kg/s) averaged between 5° S and 5° N .

In January, the PWC strengthens (weakens) in the west (east) Pacific, with positive (negative) ZMS over the west (east). Furthermore, the PWC flags westward and toward the surface (1000 hPa) in February and March. However, the PWC further heightens with westward protrusion in the upper layer over the west Pacific. This westward projection further advances in July to September, but later begins to retreat eastward in October to December.

The westward projection in June to August corresponds to the PWC strengthening reported during the monthly variation.

3.3. The Seasonal Changes in PWC Characteristics

As discussed in Section 3.2, the PWC has a periodic rhythm due to cyclical fluctuations in the exchange of energy between the atmosphere and the ocean. In this section, we examine the PWC’s seasonal variation, as indicated by the ERA5 and the NCEP2.

The position and intensity of the PWC undergo huge fluctuations on monthly to seasonal time scales; this can disrupt weather patterns around the globe. The PWC’s structure and strength also change with the season (Figure 5), which peaks (weakens) in JJA (MAM) in the tropical Pacific.

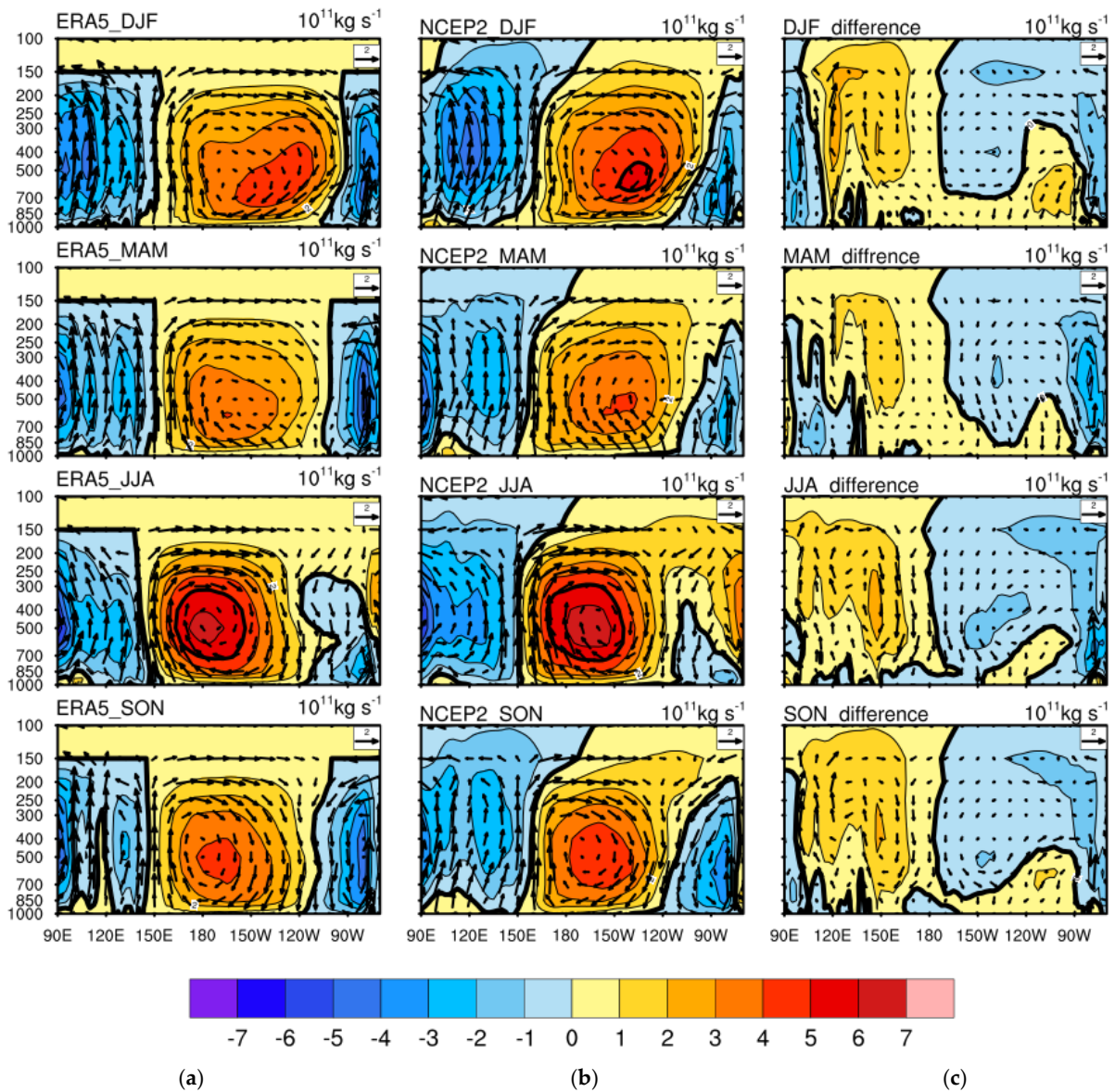


Figure 5. Seasonal climatology variation in the tropical PWC (1979–2019) in (a) ERA5, (b) NCEP2, and (c) difference (ERA5–NCEP2). Vectors are the composite of pressure velocity ($\omega \times 50; \text{Pa s}^{-1}$) and zonal divergent wind (m s^{-1}). Shading and contours represent zonal mass streamfunction (10^{11} Kg/s) averaged between 5° S and 5° N .

The PWC enhances eastward in DJF but weakens and moves westward in MAM in the east Pacific, whereas it strengthens in JJA and weakens in SON in the west Pacific. In the boreal summer, its strongest intensity and most westward extent are observed. Throughout the year, the corresponding maximum center migrates zonally.

There are also seasonal differences between the ERA5 and the NCEP2: the NCEP2 indicates higher intensity in the east Pacific during DJF and MAM (Figure 5b); how-

ever, the ERA5 indicates higher intensity in the west Pacific during boreal summer (JJA) (Figure 5a). The mean seasonal differences between the ERA5 and the NCEP2 (Figure 5c) show that the western (eastern) Pacific is influenced by a positive (negative) ZMS. The positive (negative) trend in the west (east) Pacific is at the peak in SON (JJA). This indicates that the ERA5 (NCEP2) is stronger (weaker) in JJA, whereas the ERA5 (NCEP2) is weaker (stronger) in SON.

This work is consistent with the results of [43], who discovered considerable seasonal fluctuations in the tropical PWC as a result of seasonality in the energy exchange between the atmosphere and the ocean.

3.4. Long-Term Changes of the PWC Characteristics in Reanalysis and CMIP6

The PWC structural aspects assessed by the ERA5 and NCEP2 showed similar patterns of correlation of ZMS over the equatorial Pacific, indicating that the PWC's strengthening and westward shift is seasonally dependent. In Figure 6, we compared the long-term mean annual zonal mass streamfunction (ZMS), corresponding zonal divergent winds, and vertical winds derived from the reanalysis datasets (ERA5 and NCEP2) and CMIP6. The mean-state vertical structures (Figure 6c) of the tropical PWC in the CMIP6 multi-model ensemble (MME) mean are similar to those of the reanalysis (Figure 6a,b) in structure but different in magnitude. The PWC has its core near the center of the central Pacific (150° W) and lies in the middle troposphere (between 700 and 500 hPa). Its constant streamfunction lines are denser over the regions approximately 137° E and 100° W; they are consistent with a strong ascending motion on the Maritime Continent and the western Pacific and a descending motion on the eastern Pacific, respectively. Though the CMIP6 model is able to simulate the main climatological features, it underestimates PWC intensity. Moreover, the PWC is broader in CMIP6 and the western boundary is 7 degrees farther west than in the reanalysis.

To evaluate PWC changes, we compared the PWC western edge index derived from the reanalysis products and CMIP6 in Figure 6d. The PWC western edge in the reanalysis and CMIP6 are comparable; however, the CMIP6 PWC western edge is farther westward and has a smaller change range, making it incapable of reproducing the PWC basic structure and long-term variability as captured in the reanalysis.

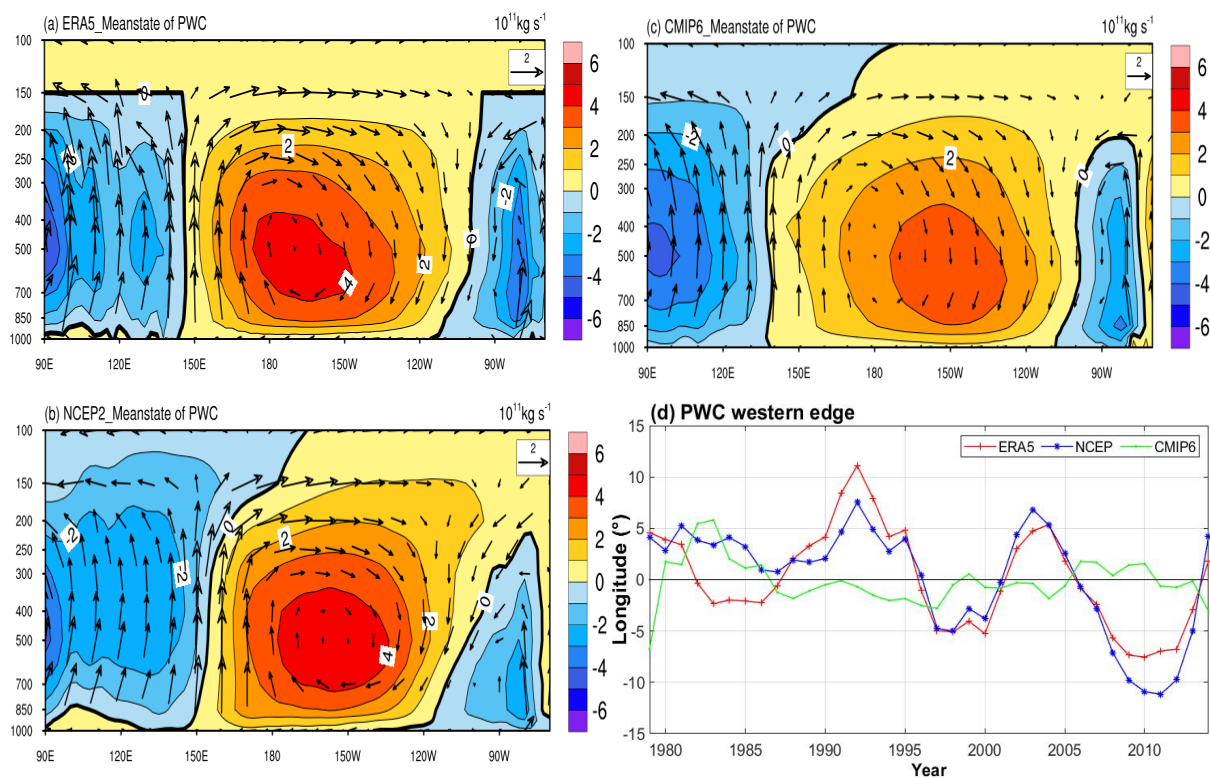


Figure 6. Mean state (1979–2014) of the tropical PWC in (a) ERA5, (b) NCEP2, (c) CMIP6, and (d) western edge ($^{\circ}$ lon), derived by applying 3-year running mean to the annual anomalies. Vectors are the composite of pressure velocity ($\omega x - 50$; Pa s^{-1}) and zonal divergent wind (m s^{-1}). Shading and contours represent zonal mass streamfunction (10^{11} Kg/s) averaged between 5° S and 5° N.

4. Discussion

The Pacific Walker circulation regulates the global heat energy budget, momentum, and water vapor within the tropics and plays a decisive role in preserving atmospheric energy. Previous studies have found significant inconsistency in model reanalyses over the equatorial Pacific [34,35]. Biases between reanalysis and climate models may misrepresent the true variation and provide inaccurate results. Atmospheric circulation in a reanalysis dataset is the best estimate of true atmospheric circulation because the zonal and meridional winds are directly assimilated from observational data [36]. However, it is worth noting that there are some slight changes in divergent circulation depicted by various reanalyses due to individual model characterization, e.g., the integration system, satellite data handling, vertical and horizontal resolution, and convective parameterizations. As a result, the global monsoon precipitation [44] and the atmospheric water vapor transport for summer precipitation over the Qinghai–Tibetan Plateau [45] derived from different reanalysis datasets differ. NCEP and ERA are the most often utilized reference datasets for testing climate models utilizing reanalysis datasets [32,37].

In Figure 7, we show the monthly (seasonal) longitude profile of PWC with zonal mass streamfunction over the tropical Pacific from 1979 to 2019. In the PWC’s structural features examined by the ERA5 and the NCEP2, the patterns’ correlation of the ZMS over the equatorial Pacific are identical. Figure 7a,b shows the seasonal variation in the PWC as depicted by the ERA5 and the NCEP2. The PWC’s strength, depicted by the maximum of the vertically averaged ZMS, is stronger in boreal summer and winter than in spring and fall, and the corresponding maximum center migrates zonally throughout the year. The PWC west edge (the zero line) migrates notably from west of about 160° E to the east in the winter (December–February) and autumn (September–November), then back to west in the spring (March–May) and boreal summer (June–August).

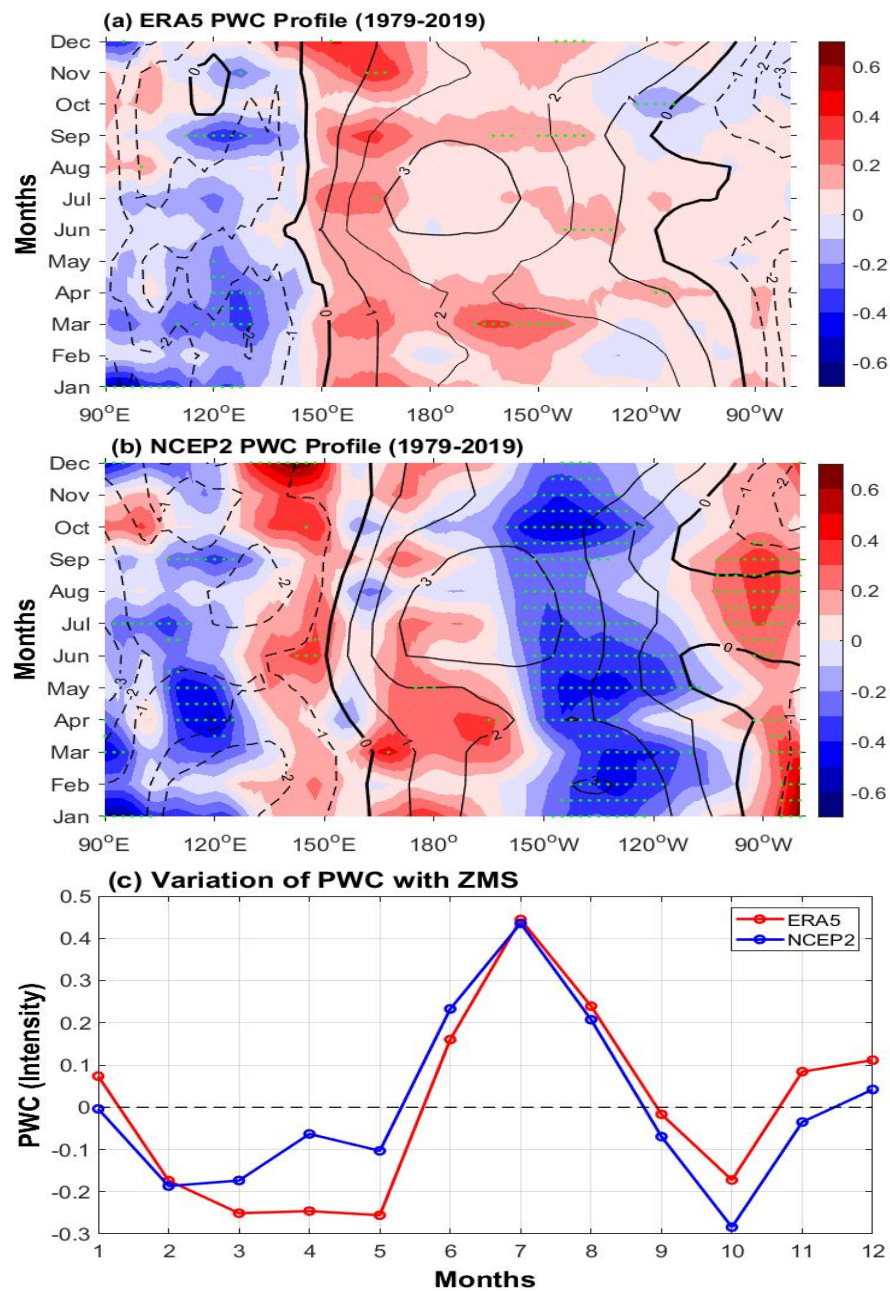


Figure 7. Monthly longitude profile of PWC with zonal mass streamfunction over the tropical (5° S– 5° N, 80° E– 280° E), 850 hPa–200 hPa for (a) ERA5, (b) NCEP2, and (c) the monthly variation in PWC with ZMS for the ERA5 and the NCEP2 derived by applying a 3-year running mean to the annual anomalies. Contours (long-term mean) and shading (linear trends) represent zonal mass streamfunction (10^{11} Kg/s) averaged between 5° S and 5° N, 850 hPa–200 hPa. Trends statistically significant at the 5% level are dotted in green.

Figure 7c shows the climatological monthly mean fluctuation of the PWC expressed in the units of vertically averaged ZMS by the ERA5 and the NCEP2. Both reanalyses reveal a similar variation pattern. The ZMS peaks in July in both reanalyses and then gradually declines, with the lowest value in October (May) in the NCEP2 (ERA5). After May, the ZMS steadily rises and peaks in July, showing that the value of the PWC is higher in the summer and lower in the autumn.

The PWC’s strengthening is consistent with the periodic evolution of cold water over the equatorial eastern Pacific, as well as the increased sea surface temperature gradient

across the Pacific. In this study, we showed that the position and intensity of the descending and ascending branches of the PWC exhibit seasonal variation. In the boreal summer, the ascending and descending branches are at their strongest, and in the spring, they are at their weakest. The corresponding maximum centers of the rising and sinking motions are likewise found to migrate zonally. This is consistent with the results of [46], who highlighted considerable seasonal fluctuation in the tropical PWC as a result of seasonality in the energy exchange between the atmosphere and the ocean. Furthermore, we show that the recent robust strengthening and westward shift of the PWC is seasonally dependent. This recent PWC intensification and westward shift contribute greatly to the observed moistening over the Indo-Pacific warm pool and drying (cooling) over the central (eastern) tropical Pacific. This differs from the findings of [4,6,28,47,48], which reported an observed and simulated twentieth-century weakening of PWC because of global warming.

5. Summary

Based on the comparison of the PWC structures between the ERA5 and the NCEP2 data using the zonal mass streamfunction, many discrepancies are identified over the equatorial Pacific between 1979 and 2019. In the NCEP2 (ERA5), the PWC is stronger and wider, with a ZMS of $5 \times 10^{11} \text{ Kgs}^{-1}$ ($4 \times 10^{11} \text{ Kgs}^{-1}$) for the circulation center. In the ERA5, the western edge (zero line of ZMS over the western Pacific) and core of the PWC were farther west by 5° and 10° than in the NCEP2. The mean state difference between the ERA5 and the NCEP2 shows that the western (eastern) Pacific is controlled by a positive (negative) ZMS, meaning that the PWC's intensity was weaker (stronger) in the ERA5 (NCEP2) reanalysis. The trend analysis revealed that positive (negative) ZMSs control the west (east) Pacific in the NCEP2, whereas positive trends dominate the whole Pacific in the ERA5. The PWC's average monthly or seasonal cycle peaks around July. From February to June, the NCEP2 shows a higher PWC intensity, whereas the ERA5 shows greater intensity from July to December. The circulation center in the NCEP2 is largely stronger and wider than in the ERA5. The ERA5 however, revealed that the PWC's west edge (zero line of ZMS over the western Pacific) moved 10 degrees westward in comparison to the NCEP2. Further comparison of the PWC's mean state in the reanalysis (ERA5 and NCEP2) and CMIP6 models showed a similar but weaker and broader PWC structure. The PWC is broader in CMIP6, and the western boundary is 7 and 17 degrees farther west than in the ERA5 and NCEP2, respectively. Thus, caution is recommended when utilizing the reanalysis datasets to evaluate PWC structural changes in intensity and western edge over the equatorial Pacific.

Author Contributions: Conceptualization, Y.G.; methodology, E.O.E.; software, E.O.E.; validation, Y.G., and E.O.E.; formal analysis, E.O.E.; investigation, Y.G. and E.O.E.; resources, E.O.E.; data curation, E.O.E.; writing—original draft preparation, E.O.E. and Y.G.; writing—review and editing, Y.G.; visualization, E.O.E.; supervision, Y.G.; project administration, Y.G. and E.O.E.; funding acquisition, Y.G. Both authors have read and agreed to the published version of the manuscript.

Funding: This study was supported by the China National Key R&D Program grant 2018YFC1506903, Key Special Project for Introduced Talents Team of Southern Marine Science and Engineering Guangdong Laboratory (Guangzhou) (GML2019ZD0306), and The World Academy of Science (TWAS) CAS-TWAS President's Fellowship (2018A8006912001), the Chinese Academy of Science (CAS).

Institutional Review Board Statement: Not applicable.

Informed Consent Statement: Not applicable.

Data Availability Statement: The data used in this research are available datasets of the National Centers for Environmental Prediction NCEP–U.S. Department of Energy reanalysis (NCEP-2; <http://www.esrl.noaa.gov/psd/data/gridded/data.ncep%20reanalyses2.html> (accessed on 14 September 2021)) and the fifth generation ECMWF reanalysis for the global climate and weather (Era5; <https://cds.climate.copernicus.eu/cdsapp#!/home> (accessed on 14 September 2021)).

Acknowledgments: The authors appreciate the National Centers for Environmental Prediction NCEP–U.S. Department of Energy reanalysis (NCEP-2), the European Centre for Medium-Range Weather Forecasts (ECMWF) and the Coupled Model Inter-comparison Project (CMIP) Phase 6 for providing the datasets used in this research. We also thank the three anonymous reviewers for helpful comments and suggestions.

Conflicts of Interest: The authors declare no conflict of interest.

References

1. Walker, G.T. Correlations in seasonal variations of weather. Part VIII: A preliminary study of world weather. *Mem. Indian Meteorol. Dep.* **1923**, *24*, 75–131.
2. Philander, S.G. *El Niño, La Nina and the Southern Oscillation*; Academic Press: New York, NY, USA, 1990; Volume 289.
3. Bjerknes, J. Atmospheric teleconnections from the equatorial pacific. *Mon. Weather Rev.* **1969**, *97*, 163–172. [[CrossRef](#)]
4. Vecchi, G.A.; Soden, B.; Wittenberg, I.A.; Held, I.M.; Leetmaa, A.; Harrison, M.J. Weakening of tropical Pacific atmospheric circulation due to anthropogenic forcing. *Nature* **2006**, *441*, 73–76. [[CrossRef](#)]
5. Gastineau, G.; Li, L.; Le Treut, H.L. The Hadley and Walker circulation changes in global warming conditions described by idealized atmospheric simulations. *J. Clim.* **2009**, *22*, 3993–4013. [[CrossRef](#)]
6. Power, S.B.; Smith, I.N. Weakening of the Walker Circulation and apparent dominance of El Niño both reach record levels, but has ENSO really changed? *Geophys. Res. Lett.* **2007**, *34*, L18702. [[CrossRef](#)]
7. Bach, E.; Motesharrei, S.; Kalnay, E.; Ruiz-Barradas, A. Local atmosphere–ocean predictability: Dynamical origins, lead times, and seasonality. *J. Clim.* **2019**, *32*, 7507–7519. [[CrossRef](#)]
8. Yu, B.; Zwiers, F.W. Changes in equatorial atmospheric zonal circulations in recent decades. *Geophys. Res. Lett.* **2010**, *37*. [[CrossRef](#)]
9. Tanaka, H.; Ishizaki, N.; Kitoh, A. Trend and interannual variability of Walker, monsoon and Hadley circulations defined by velocity potential in the upper troposphere. *Tellus* **2004**, *56*, 250–269. [[CrossRef](#)]
10. Ma, S.; Zhou, T. Robust strengthening and westward shift of the tropical Pacific Walker circulation during 1979–2012: A comparison of 7 sets of re-analysis data and 26 CMIP5 models. *J. Clim.* **2016**, *29*, 3097–3118. [[CrossRef](#)]
11. Bayr, T.; Dommenges, D.; Martin, T.; Power, S.B. The eastward shift of the Walker Circulation in response to global warming and its relationship to ENSO variability. *Clim. Dyn.* **2014**, *43*, 2747–2763. [[CrossRef](#)]
12. Li, X.; Wang, X.; Lian, T.; Johnson, N.C.; Zhu, J.; Chang, C.-H.; Liu, H.; Wang, W. Local and remote SST variability contribute to the westward shift of the Pacific Walker circulation during 1979–2015. *Geosci. Lett.* **2021**, *8*, 1–11. [[CrossRef](#)]
13. Lu, J.; Vecchi, G.; Reichler, T. Expansion of the Hadley cell under global warming. *Geophys. Res. Lett.* **2007**, *34*. [[CrossRef](#)]
14. Deser, C.; Wallace, J.M. Large-scale atmospheric circulation features of warm and cold episodes in the tropical Pacific. *J. Clim.* **1990**, *3*, 1254–1281. [[CrossRef](#)]
15. Williams, A.P.; Funk, C. A westward extension of the warm pool leads to a westward extension of the Walker circulation, drying eastern Africa. *Clim. Dyn.* **2011**, *37*, 2417–2435. [[CrossRef](#)]
16. Bayr, T.; Latif, M.; Dommenges, D.; Wengel, C.; Harlaß, J.; Park, W. Mean-state dependence of ENSO atmospheric feedbacks in climate models. *Clim. Dyn.* **2017**, *50*, 3171–3194. [[CrossRef](#)]
17. Tian, Z.; Li, T.; Jiang, D. Strengthening and Westward shift of the Tropical Pacific Walker circulation during the Mid-Holocene: PMIP Simulation Results. *J. Clim.* **2018**, *31*, 2283–2298. [[CrossRef](#)]
18. Sulca, J. Evidence of nonlinear Walker circulation feedbacks on extreme El Niño Pacific diversity: Observations and CMIP5 models. *Int. J. Clim.* **2021**, *41*, 2934–2961. [[CrossRef](#)]
19. Yan, Q.; Korty, R.; Zhang, Z.; Brierley, C.; Li, X.; Wang, H. Large shift of the Pacific Walker Circulation across the Cenozoic. *Natl. Sci. Rev.* **2020**, *8*, 101. [[CrossRef](#)]
20. Yun, K.-S.; Timmermann, A.; Stuecker, M.F. Synchronized spatial shifts of Hadley and Walker circulations. *Earth Syst. Dyn.* **2021**, *12*, 121–132. [[CrossRef](#)]
21. Webster, P.J.; Moore, A.M.; Loschnigg, J.P.; Leben, R.R. Coupled ocean–atmosphere dynamics in the Indian Ocean during 1997–98. *Nature* **1999**, *401*, 356–360. [[CrossRef](#)]
22. Wang, B.; Liu, J.; Kim, H.-J.; Webster, P.J.; Yim, S.-Y. Recent change of the global monsoon precipitation (1979–2008). *Clim. Dyn.* **2011**, *39*, 1123–1135. [[CrossRef](#)]
23. Kosaka, Y.; Xie, S.-P. Recent global-warming hiatus tied to equatorial Pacific surface cooling. *Nature* **2013**, *501*, 403–407. [[CrossRef](#)] [[PubMed](#)]
24. Liu, J.; Wang, B.; Cane, M.A.; Yim, S.-Y.; Lee, J.-Y. Divergent global precipitation changes induced by natural versus anthropogenic forcing. *Nat. Cell Biol.* **2013**, *493*, 656–659. [[CrossRef](#)]
25. England, M.; McGregor, S.; Spence, P.; Meehl, G.A.; Timmermann, A.; Cai, W.; Gupta, A.S.; McPhaden, M.J.; Purich, A.; Santoso, A. Recent intensification of wind-driven circulation in the Pacific and the ongoing warming hiatus. *Nat. Clim. Chang.* **2014**, *4*, 222–227. [[CrossRef](#)]
26. McGregor, S.; Timmermann, A.; Stuecker, M.; England, M.; Merrifield, M.; Jin, F.-F.; Chikamoto, Y. Recent Walker circulation strengthening and Pacific cooling amplified by Atlantic warming. *Nat. Clim. Chang.* **2014**, *4*, 888–892. [[CrossRef](#)]
27. Guan, X.; Huang, J.; Guo, R.; Lin, P. The role of dynamically induced variability in the recent warming trend slowdown over the Northern Hemisphere. *Sci. Rep.* **2015**, *5*, 12669. [[CrossRef](#)]

28. Power, S.B.; Kociuba, G. What Caused the Observed Twentieth-Century Weakening of the Walker Circulation? *J. Clim.* **2011**, *24*, 6501–6514. [[CrossRef](#)]
29. DiNezio, P.N.; Clement, A.C.; Vecchi, G.; Soden, B.; Kirtman, B.P.; Lee, S.-K. Climate Response of the Equatorial Pacific to Global Warming. *J. Clim.* **2009**, *22*, 4873–4892. [[CrossRef](#)]
30. Sohn, B.J.; Yeh, S.-W.; Schmetz, J.; Song, H.-J. Observational evidences of Walker circulation change over the last 30 years contrasting with GCM results. *Clim. Dyn.* **2012**, *40*, 1721–1732. [[CrossRef](#)]
31. Wang, B.; Liu, J.; Kim, H.-J.; Webster, P.J.; Yim, S.-Y.; Xiang, B. Northern Hemisphere summer monsoon intensified by mega-El Niño/southern oscillation and Atlantic multidecadal oscillation. *Proc. Natl. Acad. Sci. USA* **2013**, *110*, 5347–5352. [[CrossRef](#)]
32. Thompson, D.; Cole, J.E.; Shen, G.T.; Tudhope, A.W.; Meehl, G.A. Early twentieth-century warming linked to tropical Pacific wind strength. *Nat. Geosci.* **2014**, *8*, 117–121. [[CrossRef](#)]
33. Inoue, T.; Matsumoto, J. A comparison of summer sea level pressure over East Eurasia between NCEP-NCAR Reanalysis and ERA-40 for the period 1960–1999. *J. Meteorol. Soc. Japan* **2004**, *82*, 951–958. [[CrossRef](#)]
34. Wu, R.; Kinter, J.L.; Kirtman, B.P. Discrepancy of interdecadal changes in the Asian region among the NCEPNCAR reanalysis, objective analyses, and observations. *J. Clim.* **2005**, *18*, 3048–3067. [[CrossRef](#)]
35. Li, G.; Xie, S.-P. Tropical Biases in CMIP5 Multimodel ensemble: The excessive Equatorial Pacific cold tongue and double ITCZ problems*. *J. Clim.* **2014**, *27*, 1765–1780. [[CrossRef](#)]
36. Li, G.; Jian, Y.; Yang, S.; Du, Y.; Wang, Z.; Li, Z.; Zhuang, W.; Jiang, W.; Huang, G. Effect of excessive equatorial Pacific cold tongue bias on the El Niño-Northwest Pacific summer monsoon relationship in CMIP5 multi-model ensemble. *Clim. Dyn.* **2018**, *52*, 6195–6212. [[CrossRef](#)]
37. Kalnay, E.; Kanamitsu, M.; Kistler, R.; Collins, W.; Deaven, D.; Gandin, L.; Iredell, M.; Saha, S.; White, G.; Woollen, J.; et al. The NCEP/NCAR 40-Year Reanalysis Project. *Bull. Am. Meteorol. Soc.* **1996**, *77*, 437–471. [[CrossRef](#)]
38. Kumar, K.K.; Rajagopalan, B.; Cane, M.A. On the Weakening Relationship Between the Indian Monsoon and ENSO. *Science* **1999**, *284*, 2156–2159. [[CrossRef](#)] [[PubMed](#)]
39. Kanamitsu, M.; Ebisuzaki, W.; Woollen, J.; Yang, S.-K.; Hnilo, J.J.; Fiorino, M.; Potter, G.L. NCEP-DOE AMIP-II Reanalysis (R-2). *Bull. Am. Meteorol. Soc.* **2002**, *83*, 1631–1644. [[CrossRef](#)]
40. Hersbach, H.; Bell, B.; Berrisford, P.; Biavati, G.; Horányi, A.; Muñoz Sabater, J.; Nicolas, J.; Peubey, C.; Radu, R.; Rozum, I.; et al. *ERA5 Monthly Averaged Data on Pressure Levels from 1979 to Present*; Copernicus Climate Change Service (C3S) Climate Data Store (CDS): Bonn, Germany, 2019. [[CrossRef](#)]
41. Eyring, V.; Bony, S.; Meehl, G.A.; Senior, C.A.; Stevens, B.; Stouffer, R.J.; Taylor, K.E. Overview of the Coupled Model Intercomparison Project Phase 6 (CMIP6) experimental design and organization. *Geosci. Model Dev.* **2016**, *9*, 1937–1958. [[CrossRef](#)]
42. Bretherton, C.S.; Widmann, M.; Dymnikov, V.P.; Wallace, J.M.; Bladé, I. The effective number of spatial degrees of freedom of a time-varying field. *J. Clim.* **1999**, *12*, 1990–2009. [[CrossRef](#)]
43. Sandeep, S.; Stordal, F.; Sardeshmukh, P.D.; Compo, G. Pacific Walker Circulation variability in coupled and uncoupled climate models. *Clim. Dyn.* **2014**, *43*, 103–117. [[CrossRef](#)]
44. Schwendike, J.; Govekar, P.; Reeder, M.J.; Wardle, R.; Berry, G.J.; Jakob, C. Local partitioning of the overturning circulation in the tropics and the connection to the Hadley and Walker circulations. *J. Geophys. Res. Atmos.* **2014**, *119*, 1322–1339. [[CrossRef](#)]
45. Lin, R.; Zhou, T.; Qian, Y. Evaluation of Global Monsoon Precipitation Changes based on Five Reanalysis Datasets. *J. Clim.* **2014**, *27*, 1271–1289. [[CrossRef](#)]
46. Feng, L.; Zhou, T. Water vapor transport for summer precipitation over the Tibetan Plateau: Multidata set analysis. *J. Geophys. Res. Space Phys.* **2012**, *117*. [[CrossRef](#)]
47. Yu, B.; Zwiers, F.W.; Boer, G.J.; Ting, M.F. Structure and variances of equatorial zonal circulation in a multimodel ensemble. *Clim. Dyn.* **2012**, *39*, 2403–2419. [[CrossRef](#)]
48. Knutson, T.R.; Manabe, S. Time-mean response over the tropical Pacific to increase CO₂ in a coupled ocean–atmosphere model. *J. Clim.* **1995**, *8*, 2181–2199. [[CrossRef](#)]